**PSFC/JA-08-46**

# Studies of turbulence and transport in Alcator C-Mod H-Mode plasmas with phase contrast imaging and comparisons with GYRO

L. Lin[1], M. Porkolab[1], E.M. Edlund[1], C. Fiore[1], M. Greenwald[1], Y. Lin[1], D. Mikkelsen[2], J.C. Rost[1] and S.J. Wukitch[1]

June 2009

**Plasma Science and Fusion Center**
**Massachusetts Institute of Technology**
**Cambridge MA 02139 USA**

[1]*M.I.T. Plasma Science and Fusion Center - Cambridge, Massachusetts 02139*

[2]*Princeton Plasma Physics Laboratory – Princeton, NJ 08543*

This work was supported by the U.S. Department of Energy, Grant No. DE-FC02-99ER54512. 

Submitted for publication to *Physics of Plasmas.*

# Studies of turbulence and transport in Alcator C-Mod H-Mode plasmas with phase contrast imaging and comparisons with GYRO

**L. Lin[1], M. Porkolab[1], E.M. Edlund[1], J.C. Rost[1], C.L. Fiore[1], M. Greenwald[1], Y. Lin[1], D.R. Mikkelsen[2], N. Tsujii[1], and S.J. Wukitch[1]**

*[1]Plasma Science and Fusion Center, Massachusetts Institute of Technology, Cambridge, MA 02139*

*[2]Princeton Plasma Physics Laboratory, Princeton, New Jersey 08543*

**Abstract—**Recent advances in gyrokinetic simulation of core turbulence and associated transport requires an intensified experimental effort to validate these codes using state of the art synthetic diagnostics to compare simulations with experimental data. A phase contrast imaging (PCI) diagnostic [M. Porkolab, J.C. Rost, N. Basse *et al*., IEEE Trans. Plasma Sci. **34**, 229 (2006)] is used to study H-Mode plasmas in Alcator C-Mod [M. Greenwald, D. Andelin, N. Basse *et al*., Nucl. Fusion **45,** S109 (2005)]. The PCI system is capable of measuring density fluctuations with high temporal (2 kHz-5 MHz) and wavenumber (0.5-55 $cm^{-1}$) resolution. Recent upgrades have enabled PCI to localize the short wavelength turbulence in the electron temperature gradient (ETG) range and resolve the direction of propagation (i.e., electron vs. ion diamagnetic direction) of the longer wavelength turbulence in the ion temperature gradient (ITG) and trapped electron mode (TEM) range. The studies focus on plasmas before and during internal transport barrier formation in an enhanced $D_\alpha$ H-Mode plasma assisted with ion cyclotron resonance frequency (ICRF) heating. Nonlinear GYRO simulations have also been performed [J. Candy and R. E. Waltz, Phys. Rev. Lett. **91**, 045001 (2003)] and the predicted fluctuation is compared against experimental measurements through a synthetic PCI diagnostic method. The simulated fluctuations from GYRO agree with experimental measurements in the ITG regime. GYRO also shows good agreement in transport predictions with experimental measurements after reducing the ion temperature gradient (~15%) and adding E×B shear suppression, all within the experimental uncertainty.

## I. INTRODUCTION

While comprehensive theoretical models and simulations have been developed to the stage of being able to quantitatively predict turbulence and transport in fusion plasmas[1-5], detailed experimental comparisons and validations remain a challenge. Comparisons of simulated turbulence with experimental measurements are difficult because turbulence diagnostics are limited by system response and do not exactly measure the quantities being simulated. One

approach to resolve this issue is through the use of a "virtual diagnostic"[6] built into the output of numerical simulation to emulate diagnostic measurements with proper system response and sensitivity included.

The phase contrast imaging diagnostic (PCI) in Alcator C-Mod[7] has been used to study drift-wave type turbulence. However, the previous studies were limited to experimental observation[8], or at best a qualitative comparison with numerical simulation[9]. The recent development of an improved calibration for the PCI system allows for the intensity of the observed fluctuations to be determined absolutely.[10] Furthermore, development of the synthetic PCI diagnostic[11] on GYRO[1] allow for direct and quantitative comparisons between the PCI measurements and numerical predictions. In this paper, we present studies of turbulence and transport in C-Mod H-Mode plasmas using the calibrated PCI and synthetic diagnostic tools. We also examine H-Mode plasmas with internal transport barriers (ITBs) assisted with ion cyclotron resonance frequency (ICRF) heating.[12] Because of its reduced energy and/or particle transport and improved confinement, understanding ITB physics remains of great interest to the fusion community. Our studies focus on the plasma both before and after the ITB formation as on and off-axis ICRF heating is applied.

This paper is organized as follows: in Sec. II, the experimental setup is presented; in Sec. III, fluctuation measurements are presented; in Sec. IV, the gyrokinetic simulation of turbulence and transport is discussed; in Sec. V, a comparison is given between fluctuation measurements and GYRO predictions. Finally, in Sec. VI the conclusions are presented.

## II. Experimental Setup

Alcator C-Mod[13] is a compact (major radius $R_0$=0.67 m and minor radius a=0.22 m) and diverted tokamak with molybdenum-facing components with the capabilities to operate at high toroidal magnetic field $B_\phi$ (up to 8.0 T), high plasma current $I_P$ (up to 2 MA), and high averaged electron density $\bar{n}_e$ (up to $6\times10^{20}$ $m^{-3}$). The primary auxiliary heating in C-Mod is RF waves in ion cyclotron range of frequencies (ICRF) launched by two 2-strap antennas at 80 MHz and one 4-strap antenna with a tunable frequency from 50 to 80 MHz, which can provide an input power up

to 6 MW.[14] For the case studied here, the ICRF antennas are configured for hydrogen minority resonance heating in deuterium majority plasmas.

The experiments considered here were conducted with the on-axis toroidal magnetic 4.5 T and the plasma current 0.8 MA. Time traces of the major parameters of a typical plasma discharge are shown in Fig. 1. At t=0.8 sec, the EDA H-Mode[15] is fully developed, following application of the off-axis (r/a=0.5) ICRF heating of 2.0 MW at 80 MHz on the high field side starting at t=0.7 sec. After another ~0.28 sec, an ITB is established at t=1.08 sec, manifesting itself in steepened density profiles (see Fig. 2). Earlier experiments found that impurities accumulate in the plasma core after the ITB formation, which can lead to a radiative collapse of the transport barrier.[16] To control the impurity accumulation and maintain the steady ITB, an additional on-axis (r/a=0.1) ICRF heating power of 0.6 MW at 70 MHz is added.[17] This added on-axis ICRF heating arrests the density rise, as shown in Fig. 1(c), where the line-integrated density ceases to increase after the on-axis heating is added. As a result, the ITB lasts for another ~0.3 sec until the end of the ICRF heating pulse at t=1.5 sec. The on-axis ICRF heating also causes a near-doubling of the fusion neutron rate, as shown in Fig. 1(b). In addition, the intensity of the $D_\alpha$ emission increases after the on-axis ICRF heating is added, which suggests an impact of the extra on-axis heating on plasma edge turbulence.

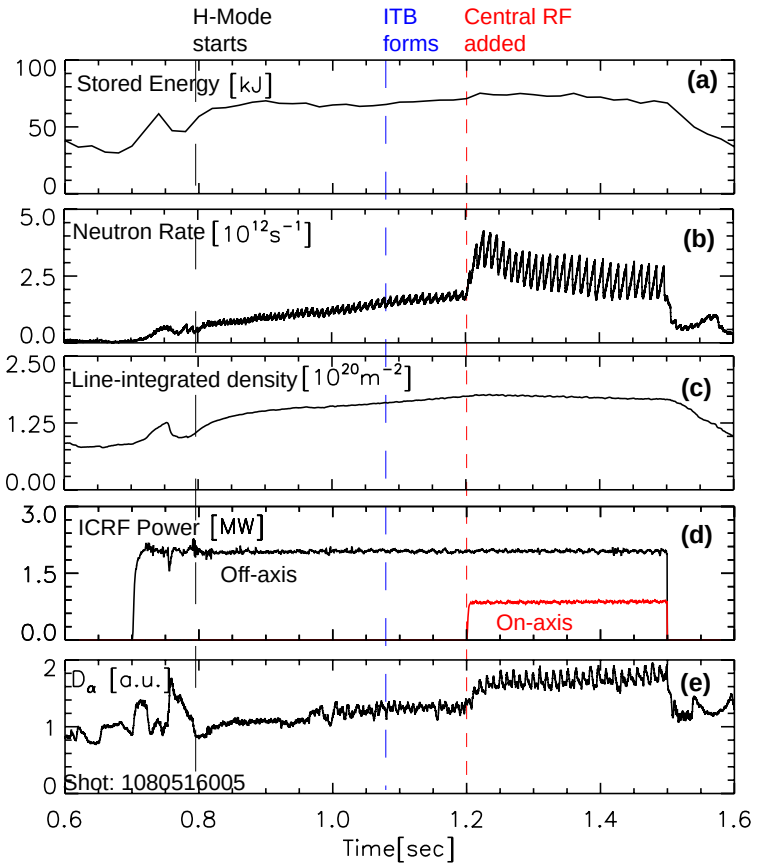


**Fig. 1.** (Color online). Plasma parameters for the studied discharge: (a) store energy; (b) neutron rate; (c) line-integrated electron density; (d) ICRF power; (e) Dα light.

The ITB plasmas in Alcator C-Mod feature a peaked electron density profile, as shown in Fig. 2(a), while the induced change in the electron temperature profiles during ITB is much less pronounced (see Fig. 2b). At such high electron density, the electrons and ions are strongly coupled due to collisions and $T_i \simeq T_e$.

We also want to point out that the experimental features of ITB in the considered plasmas are not very apparent. Our later transport analysis (Fig. 8) in Sec. V shows that the effective thermal diffusivity drops from $0.4\ \mathrm{m}^2/\mathrm{sec}$ to $0.2\ \mathrm{m}^2/\mathrm{sec}$ at $r/a = 0.5$ after the ITB onset, which confirms the existence of an ITB.

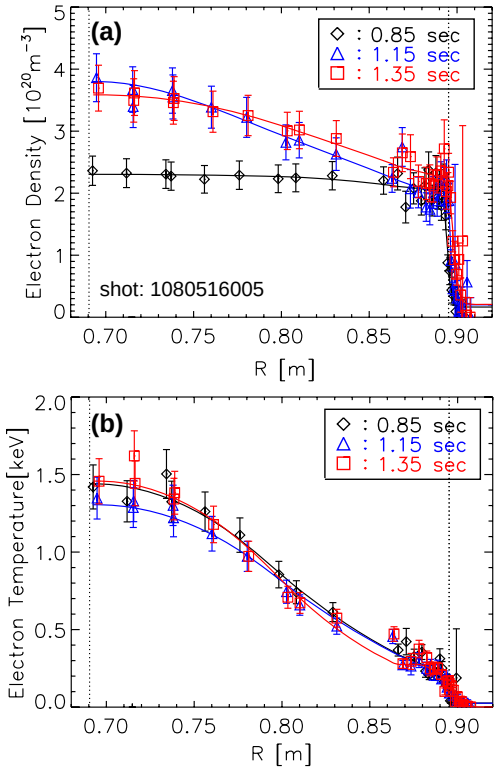


**Fig. 2.** (Color online). Profiles of electron density (a) and temperature (b) from the Thomson scattering (TS) diagnostic[18] are shown before the ITB onset (black diamond), during the ITB with only off-axis ICRF heating (blue triangle), and during the ITB after adding on-axis ICRF heating(red square). The solid line is a fit to the experimental measurements using FiTs. Two vertical dashed lines are the magnetic axis and last closed flux surface (LCFS), respectively.

## III. Fluctuation Measurements

To study the change in turbulent transport as an ITB forms, it is of great importance to measure the change in turbulent fluctuations. In Alcator C-Mod, the phase contrast imaging (PCI) diagnostic has been used to monitor these fluctuations.[7] PCI is an internal reference interferometer technique, and as shown in Fig. 3, the entire expanded $CO_2$ laser beam at 10.6μm wavelength is sent through the plasma and modulated by longer wavelength electron density fluctuations. The PCI technique relies on spatial filtering at the phase plate to additionally phase shift the reference beam (part of the $CO_2$ beam) by $\pi/2$, and this will transform phase variations $\Delta\phi \propto \int \tilde{n} dl$ in the plasma into intensity variations at the detector array. The scattered signal and reference beam are finally recombined across 32 photoconductive HgCdTe linear detectors, which provide sampling of the density fluctuations along the tokamak major radius with an effective chord spacing that is set by the magnification of the imaging optics system. The

analog signal from the detectors, after passing through the preamplifiers which provide a gain of ~200, is sent to 32 D-tacq digitizers with a sampling rate of 10 MHz. This has enabled the Alcator C-Mod PCI system to measure turbulent density fluctuations in the wavenumber range of 0.5-55 $cm^{-1}$ and in the frequency range of 2 kHz to 5 MHz. In Alcator C-Mod, the PCI system has been calibrated with a 15 kHz soundburst from an audio speaker, whose pressure fluctuations are measured with a calibrated microphone. An absolute calibration has been obtained by using the PCI system to measure the density perturbations induced by these sound waves.

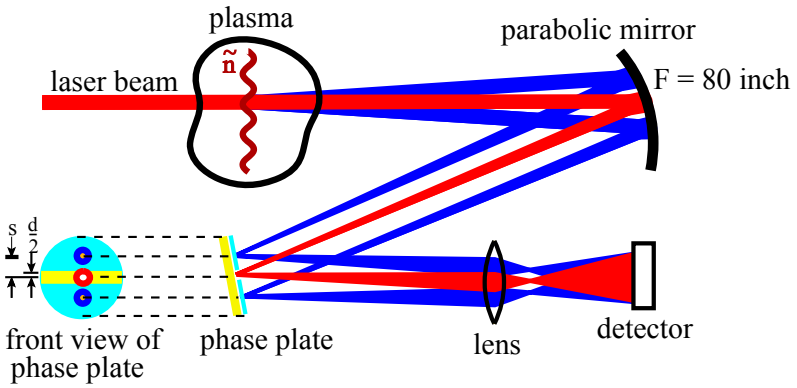


**Fig. 3.** (Color online). Principle of phase contrast imaging

Although the PCI diagnostic normally lacks localization along the chords, the vertical variation of the magnetic field pitch angle allows for some localization of short wavelength fluctuations.[19-22] The method relies on the fact that the magnetic pitch angle $\beta = \arctan(B_R / B_\phi)$ changes along a vertical chord passing through the plasma as shown in Fig. 4, where $B_R$ is the magnetic field component along the major radius and $B_\phi$ is the toroidal magnetic field. Since the wavevectors of electrostatic turbulence are mainly perpendicular to the field lines, i.e., $\mathbf{k} \cdot \mathbf{B} \approx 0$, they also rotate from the bottom to the top of the plasma as the field pitch angle rotates. This rotation is imaged onto the phase plate used in the PCI system, where we can select a vertical region of interest by partially masking specific areas of the phase plate. The localizing performance depends on the separation ($s$) between scattered beams from two different vertical regions ($z_1$ and $z_2$), where $s \propto k\Delta\beta$ and $\Delta\beta = \beta_{z1} - \beta_{z2}$. For short wavelength turbulence (large $k$), the two scattered beams are completely separated. Based on this principle, the recently installed system in C-Mod[21] consisting of a partially masked phase plate on a rotatable stage allows the PCI system to localize the short wavelength turbulence. In the longer wavelength regime in the ion

temperature gradient (ITG) and trapped electron mode (TEM) range, the localization is not as fine, but still allows for selection of the turbulence from the top (positive $z$; positive $\beta$) or the bottom (negative $z$; negative $\beta$) of the plasma, thereby resolving the direction of propagation. In addition to the direction of propagation, further analysis can also shed some light on the mode localization (core vs. edge) of the longer wavelength turbulence. Since C-Mod has a larger magnetic pitch angle in the domain of $0.3\ \text{m} > |z| > 0.1\ \text{m}$, the localizing performance is better for the turbulence coming from the plasma core than that from the plasma edge at the same wavenumbers.

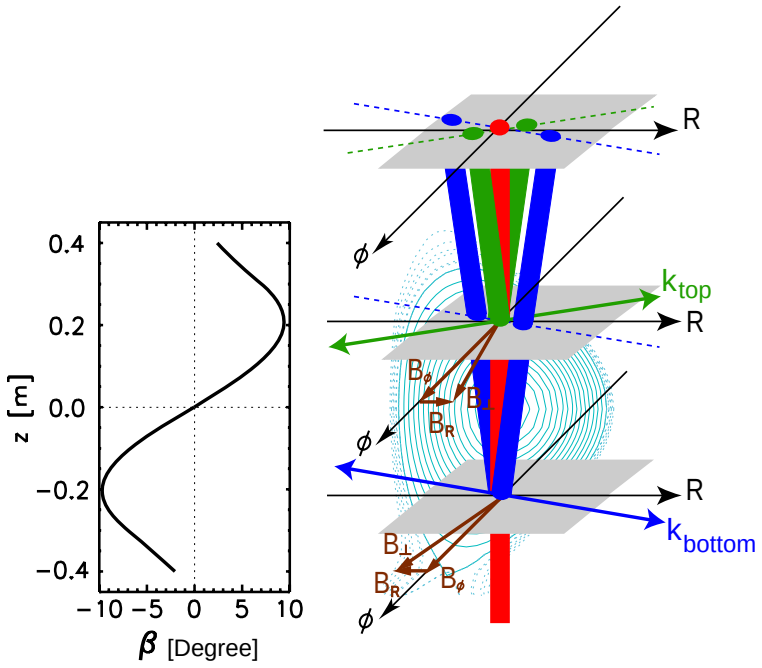


**Fig. 4.** (Color online). Left: magnetic pitch angle $\beta$ vs. vertical coordinate $z$; Right: principle of vertical localization. The red beam corresponds to the unscattered beam, while the blue (green) beam corresponds to the scattered beam from the turbulence localized at $z = -0.2$ m ($z = +0.2$ m).

Typical discharges studied in this paper exhibit broadband turbulence as well as a quasi-coherent (QC)[23] fluctuation. The spectrogram of the measured fluctuation from the single PCI chord (channel 17) is shown in Fig. 5, corresponding to the plasma evolution shown in Fig. 1. When the EDA H-Mode develops ~0.1 sec after the off-axis ICRF, the QC mode (~140 kHz) appears. The visible frequency of the broadband fluctuations increases from 250 kHz at 0.65 sec to 450 kHz at 0.90 sec. The burst at 0.75 sec was due to the unsteady ICRF heating (i.e., periodic

dropouts). The density peaking starts at ~1.0 sec and ITB forms at ~1.1 sec. During the density peaking, the intensity of broadband turbulence with frequencies below 100 kHz increases, but the upper bound of the visible frequency of broadband turbulence decreases. Since the experimentally measured frequency equals to the mode frequency plus the Doppler shift due to E×B drift velocity, i.e. $f_{lab} = f_{\text{mode}} + f_{\text{E×B}}$, the decrease of the frequency broadening suggests a corresponding change in the radial electric field. The intensities of both broadband turbulence and QC modes increase following the addition of the on-axis ICRF heating.

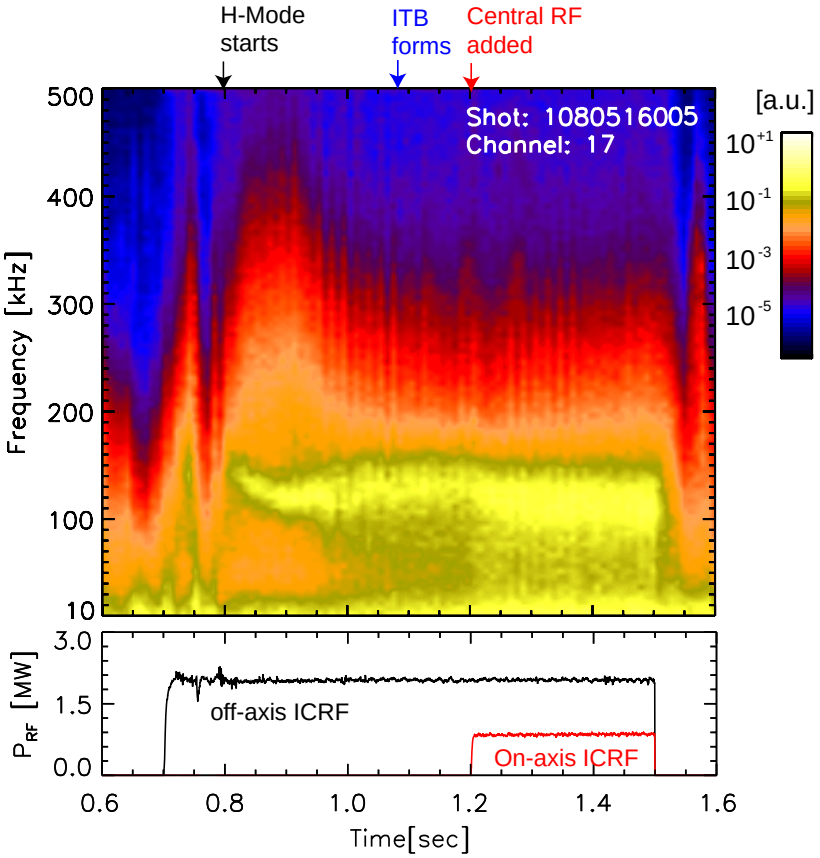


**Fig. 5**. (Color online). Main plot: Spectrogram of a core PCI channel (17) vs. time. Time resolution is 10 ms and frequency resolution is 5 kHz. Bottom plot: Traces of on-axis (black) and off-axis (red) ICRF power.

Figure 6 shows how the mode propagating direction is inferred by comparing the measured frequency/wavenumber spectra with the different localizing configurations. In Fig. 6(a), the masking plate was set up primarily to view the bottom of the plasma column, and we see that the positive wavenumber QC at frequency ~140 kHz and wavenumber ~4 $\text{cm}^{-1}$ dominates. In Fig. 6(b), the masking plate was set up mainly to view the top of the plasma column, and it is seen that the negative wavenumber QC mode dominates. This measurement agrees with the fact that

the QC mode propagates in the electron diamagnetic direction. Early studies[23] also show that the QC mode propagates perpendicular to the magnetic field just as the electrostatic turbulence, which validates the use of the localizing procedure. Similar analysis of the frequency/wavenumber spectra in Fig. 6 shows that the broadband turbulence in the frequency range of 200-500 kHz propagates in the ion diamagnetic direction.

The masking system also suppresses the broadband turbulence in the frequency range of 200-500 kHz more strongly than the QC mode. As shown in Fig. 6(b), for the top plasma view, the ratio of intensity of the broadband turbulence in the negative wavenumber to that in the positive wavenumber is 4.5, while the ratio of intensity of the QC mode in the positive wavenumber to that in the negative is 1.5. Since the top/bottom differentiation is better for the broadband turbulence than for the QC mode, the broadband turbulence has to be localized further radially inward where the magnetic pitch angle is greater (as in Fig. 4).

The PCI measurements are averaged over 0.1 sec to reduce the statistical uncertainty while turbulence is still evolving within the averaging time range, which causes the ripple patterns as shown in Fig. 6(a). The comparisons with nonlinear gyrokinetic simulations in Sec. V show that the broadband turbulence is consistent with the ITG turbulence.

The phase velocity can also be calculated from frequency/wavenumber spectra. Before the ITB formation, as in Fig. 6, the phase velocity of the broadband turbulence is ~4 km/sec. After the ITB formation, as in Fig. 7, the phase velocity of the broadband turbulence is reduced to 2 km/sec. This change of the phase velocity is due the reduction of the E×B Doppler shift.

In Alcator C-Mod, the high resolution spectroscopy (Hirex) diagnostic[24] measures density ($n_I$), temperature ($T_I$), flow velocity ($V_\theta$ and $V_\phi$) of the $Ar^{+17}$ impurity. The radial electric field ($E_r$) can be calculated through the force balance equation

$$E_r = \frac{\nabla p_I}{e n_I Z_I} - V_\theta B_\phi + V_\phi B_\theta$$

where, where $p_I = n_I T_I$. The Hirex diagnostic measures a 10±3 kV/m decrease of the radial electric field at $0.35 < r/a < 0.65$ after the ITB forms, which will cause 2±0.6 km/sec reduction

of the phase velocity of the measured fluctuation. Here, only $0.35 < r/a < 0.65$ is considered since our gyrokinetic analysis in Sec. IV shows no unstable drift-wave turbulence for $r/a < 0.35$. Moreover, since the ITB tends to create an impurity pinch and causes all the $Ar^{+17}$ impurity to accumulate in the core, there is not enough $Ar^{+17}$ left outside for the Hirex diagnostic to make the measurements. Therefore, the Hirex measurements do not extend out past $r/a = 0.65$ during the ITB, which also approve the existence of an ITB.

Because of the reduced radial electric field after the ITB formation, the reduced E×B Doppler shift is not enough to separate the core and edge turbulence in the frequency domain below 250 kHz; thus, the broadband turbulence (propagating in the ion direction in the H-mode) is mixed together with the edge localized QC modes (propagating in the electron direction). Since the intensity of the broadband turbulence is weaker than that of the QC mode, it will be overwhelmed and the PCI diagnostic cannot resolve its direction of propagation.

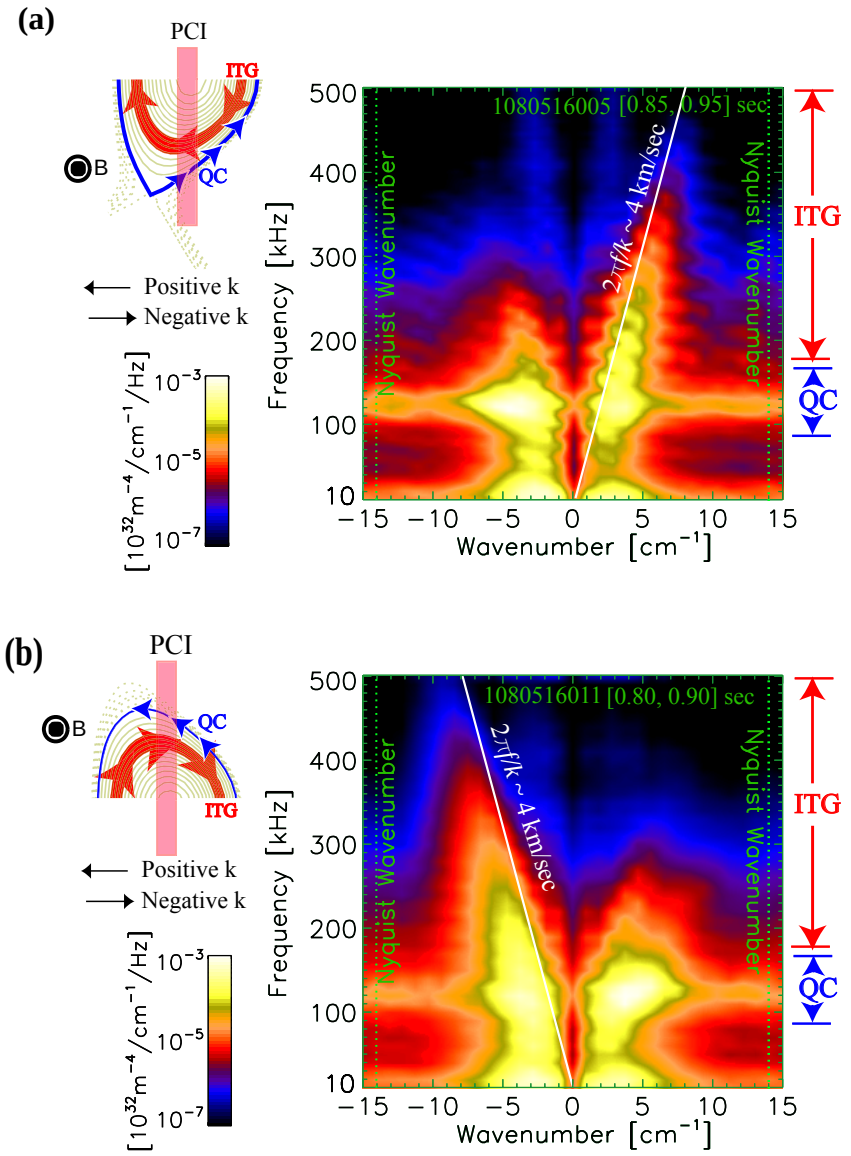


**Fig. 6**. (Color online). Frequency/wavenumber spectra of plasma fluctuations measured by PCI in the H-mode plasma before the ITB formation. On the left-corner of each plot, the diagnostic line-of-sight is shown according to the masking phase plate setup: (a) the bottom plasma view, (b) the top plasma view.

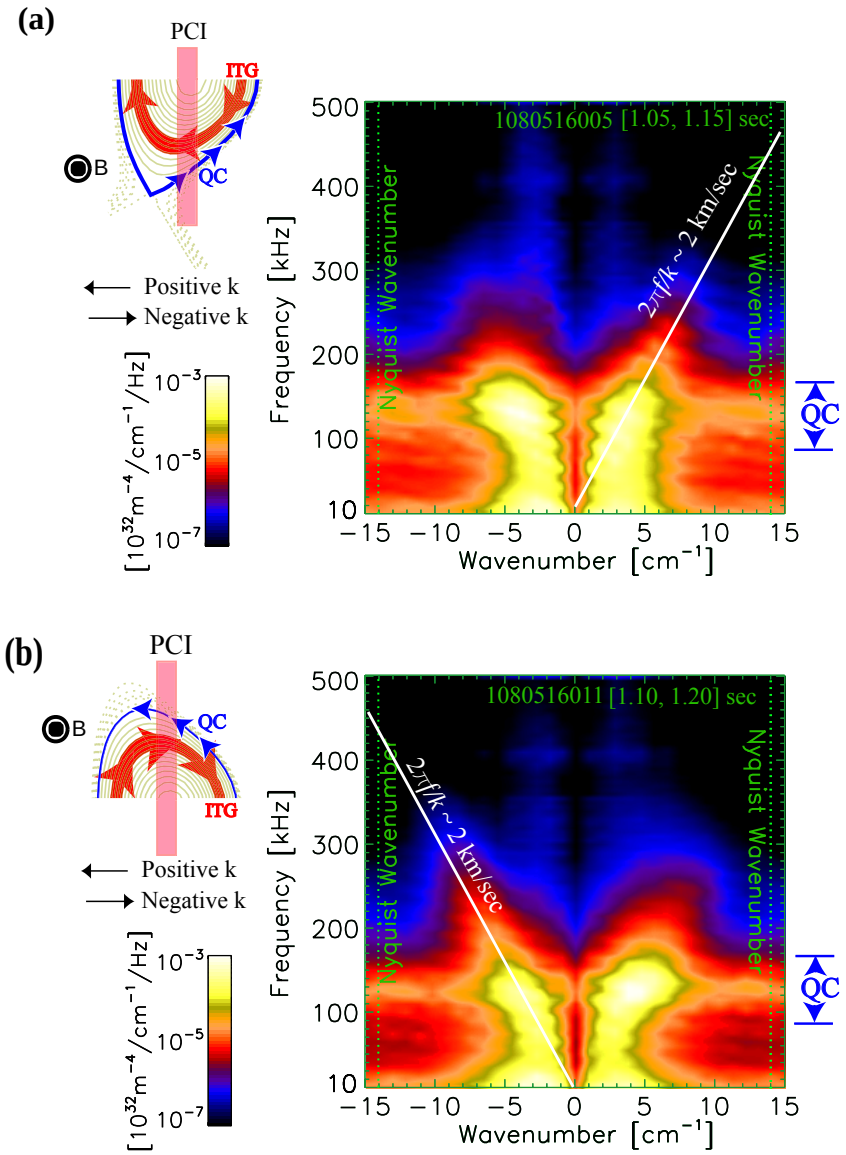


**Fig. 7**. (Color online). Frequency/wavenumber spectra of plasma fluctuations measured by PCI in the ITB plasma with only off-axis ICRF heating. On the left-corner of each plot, the diagnostic line-of-sight is shown according to the masking phase plate setup: (a) the bottom plasma view, (b) the top plasma view.

## IV. Gyrokinetic Simulation of Turbulent Transport

To further explore the nature of turbulence and the drive mechanism of thermal transport, we have used GYRO[1] to simulate turbulence and transport. GYRO[1] is a physically comprehensive global code which solves the nonlinear gyrokinetic equations for both ions and electrons. While GYRO can include electromagnetic effects, the electrostatic approximation is assumed for all the simulations here, since electromagnetic effects are negligible in low β plasmas ( $\beta \lesssim 0.3\%$ ). GYRO can take measured experimental profiles as input and solve the gyrokinetic equations in

the realistic geometry (Miller local equilibrium formulation) in an Eulerian discretization scheme. In our simulation, the input file is prepared from the output of TRANSP[25] using the data translator (trgk) developed at PPPL. Both linear stability analysis and nonlinear (local and global) simulation has been performed.

The ion temperature profile is taken to be same as the electron temperature profile (Fig. 2-b), since the electrons and ions are strongly coupled due to collisions at such high electron density. The TRANSP analysis also calculates an ion temperature profile consistent with the neutron measurement[26]. The calculated ion temperature is close to the electron temperature, which validates the assumption of $T_e = T_i$. Although the Hirex diagnostic can also measure the ion temperature profile, the measured profile does not extend out past $r/a = 0.65$ as discussed in Sec. III. However, the measured ion temperature inside $r/a = 0.65$ is close to the electron temperature, which also validates the assumption of $T_e = T_i$.

Linear stability calculation shows that the ITG mode is the most unstable mode in the plasmas before and during ITB formation. The calculated growth rate spectrum typically peaks at $k_\theta \rho_s \sim 0.4$, where $k_\theta$ is the wavenumber in the poloidal direction, $\rho_s = c_s / \Omega_i$ is the ion-sound Larmor radius, $c_s = (T_e / m_i)^{1/2}$ is the ion sound speed, $\Omega_i = eB_\Phi / (m_i c)$ is the ion cyclotron frequency, and $m_i$ is the ion mass. The frequency of the unstable modes is proportional to $k_\theta \rho_s$ and the modes propagate in the ion diamagnetic direction. The linear stability calculation also shows that the trapped electron modes (TEM) are typically stable in the plasma core even after reducing the ion temperature gradient gradually until the ITG modes are stable.

Our nonlinear GYRO simulations include $N_n$ modes with a toroidal separation of $\Delta n$. All simulations are performed with the real mass ratio ($m_i / m_e \approx 3600$) and kinetic electrons. The uncertainty of analyzing the electron thermal diffusivity $\chi_e$ and the ion thermal diffusivity $\chi_i$ separately is large when $T_i$ is close to $T_e$;[27] hence, we only discuss the effective thermal diffusivity $\chi_{eff}$ here, where $\chi_{eff} \equiv (\chi_i + \chi_e)/2$. Seven nonlinear simulations (five local and two global simulations) with no equilibrium E×B shear and no parallel velocity were performed for each case. The comparisons between the experimentally measured and simulated thermal

diffusivities are shown in Fig. 8: (a) before the ITB onset; (b) during the ITB. The simulated turbulent transport agrees well with experiments in non-ITB plasmas, while it is larger than experimental measurements in ITB plasmas with only off-axis ICRF heating. Extensive convergence studies have also been performed. As shown in Fig. 8a, the global simulations with different set of modes ( $N_n = 28$ , $\Delta n = 5$ vs. $N_n = 16$ , $\Delta n = 10$ ) agree with each other. As also shown in Fig. 8b, global simulations with different box sizes ( $480\rho_s$ vs. $320\rho_s$ ) match well in the overlapped domain $0.4 < r/a < 0.68$. Our studies also show robust consistency between nonlinear global and local flux-tube simulations at almost all radial positions.

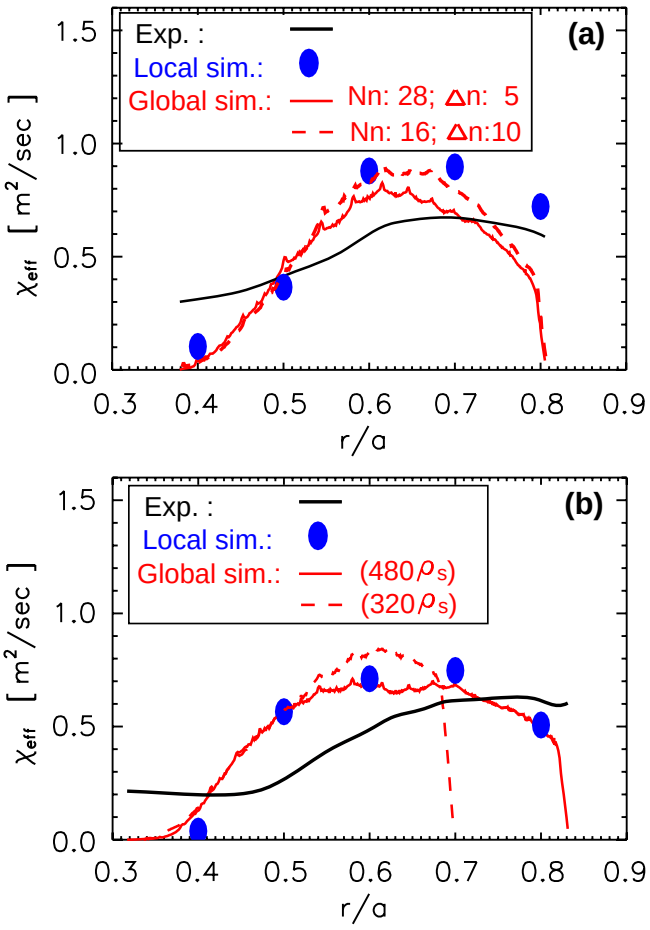


**Fig. 8.** (Color online). Comparison of experimental and nonlinearly simulated thermal diffusivities: (a) before the ITB onset; (b) during the ITB with only off-axis ICRF heating.

To further investigate the discrepancy in ITB plasmas, we have studied the impact of varying the ion temperature gradient, as is done in other studies[28]. Decreasing $a/L_{Ti} = -(a/T_i)(dT_i/dr)$ by 15%

from the baseline parameter, as shown in Fig. 9(a), is sufficient to reduce the simulated $\chi_{eff}$ to the experimental level at r/a=0.6. It is also well known that E×B shear can also suppress the simulated transport.[29] As shown in Fig. 9(b), adding ~30 kHz E×B shear lowers the simulated $\chi_{eff}$ to the experimental level. Considering the fact that experimental uncertainty of the ion temperature gradient measurements is above 20% and that E×B shear rates are not yet well measured in Alcator C-Mod, the discrepancy between the experimentally measured and simulated transport in the ITB plasma can be attributed to the experimental uncertainty.

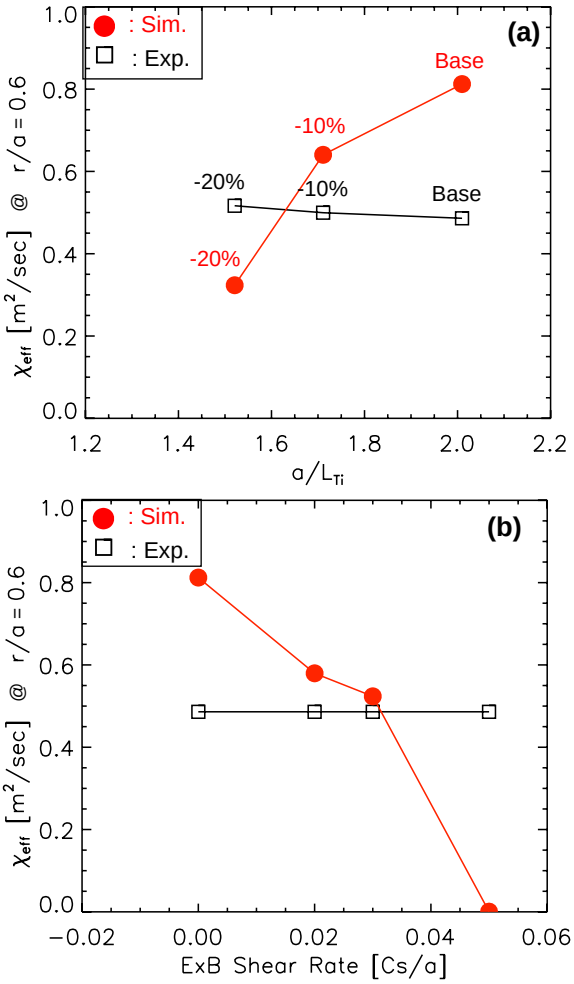


**Fig. 9.** (Color online). (a) Impact of varying a correction factor applied to the measured ion temperature gradient in the ITB plasma with only off-axis ICRF heating, where $a/L_{Ti} = -(a/T_i)(dT_i/dr)$; (b) Effect of the E×B shear on turbulent transport in the ITB plasma with only off-axis ICRF heating, where $c_s/a = 9\times10^5$ Hz.

The impact of varying density gradients on turbulent transport has also been studied. The result is shown in Fig. 10, where it is found that the density gradient variation has a weak impact on

turbulent transport. The simulated transport can only be reduced to the experimental level and the trapped electron mode (TEMs) become significant after increasing the $a/L_n = -(a/n)(dn/dr)$ by at least a factor of two, which is outside the experimental error bars based on Thomson Scattering data such as shown in Fig. 2(a). Thus, for the measured temperature and density profiles, significant transport contribution from the TEM is not likely.

We have also carried out a detailed linear stability analysis in the electron temperature gradient (ETG) regime. The unstable ETG is found with the growth rate spectra peaking at $k_\theta \rho_s \sim 25$ across the domain of r/a>0.4. Regarding transport studies, we have not had access to computer capabilities that are necessary for nonlinear GYRO simulation of such turbulence. In the future we will undertake an experimental search for high-k turbulence ($k_\theta \rho_s > 1$) in the ETG regime, which should manifest itself in higher frequency components.

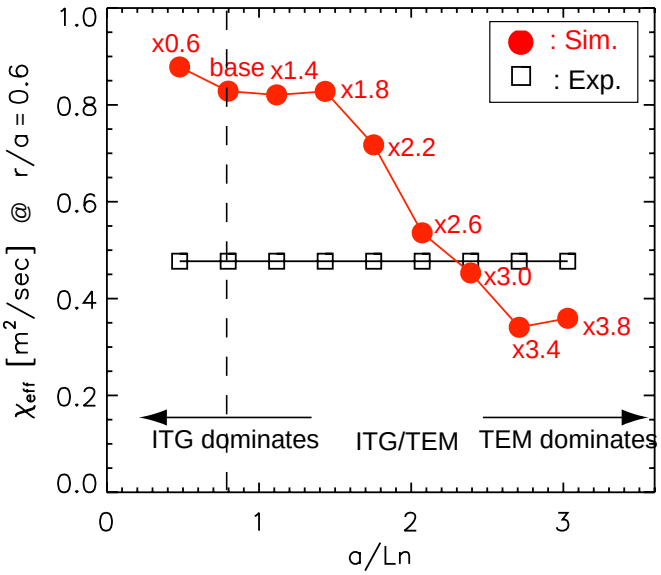


**Fig. 10.** (Color online). Impact of varying a correction factor applied to the measured density gradient on turbulent transport in the ITB plasma with only off-axis ICRF heating, where $a/L_n = -(a/n)(dn/dr)$.

## V. Comparison between Fluctuation Measurements and GYRO Prediction

Direct and quantitative comparison between experimentally measured and simulated turbulence in C-Mod is rather difficult. This is partially caused by the limited diagnostic capability and access. For example, PCI measures line-integrated density fluctuations with an instrumental limit primarily in the wavenumber response. To expedite a comparison between experiment and theory, a virtual diagnostic, known as synthetic PCI diagnostic was developed by the MIT PCI diagnostic group at DIII-D[11]. This technique has been adapted to the Alcator C-Mod PCI diagnostic configurations. The synthetic PCI analyzes the density fluctuation output of the GYRO global nonlinear simulation and emulates the experimental PCI measurements by line-integrating the density fluctuations, i.e., $\int \tilde{n}(z)dz$. Thus, it allows for a direct and quantitative comparison between numerical simulation and experimental measurements.

The synthetic PCI frequency/wavenumber diagram in the non-ITB plasma is shown in Fig. 11(a). A flat $v_{E\times B}$=4.0 km/sec has been added to account for the unmeasured Doppler shift. To emulate the top view configuration of the masked phase plate, a weight function $w(z)$ is added when performing line integral of density fluctuations, i.e., $\int w(z)\tilde{n}(z)dz$.[21,22] Comparing the synthetic PCI from Fig. 11(a) with the experimental measurement in Fig. 6(a), the intensity of the simulated turbulence is lower than the experimental measurement in the frequency below 300 kHz, where the PCI measurements begin to be dominated by the edge turbulence. However, as shown in Fig. 11(b), the fluctuation spectrum measured by PCI above 300 kHz agrees well with the ITG turbulence in GYRO simulation within experimental uncertainty, including the direction of propagation, wavenumber spectrum, and absolute intensity. GYRO only simulates one time point, where the equilibrium profiles are fixed, while the experimental measurements cover 0.1 sec. The variation of the density and temperature profiles within 0.1 sec will broaden the experimental measurements. Therefore, the synthetic PCI spectra appear to be narrower in wavenumber than the experimental spectra. Moreover, in the synthetic PCI analysis, a flat $v_{E\times B}$ is introduced to account for the unmeasured Doppler shift. The potential variation of $v_{E\times B}$ along the integration chord will also cause a different Doppler shift for the turbulence with the same wavenumber, thereby broadening the experimental spectra.

After the ITB formation, the core and edge turbulence is mixed together on PCI due to the reduced E×B Doppler shift; thus, as shown in Fig. 12, the synthetic PCI spectra (the base case simulation with no reduction of the ion temperature gradient or E×B shear suppression), where $v_{E\times B}$=2.0 km/sec has been added for the Doppler shift, shows weaker fluctuation intensity than the PCI measurements (Fig. 7(a)) which also include contributions from the plasma edge.

These comparisons show that, when there is sufficient E×B Doppler shift, the fluctuation measurements by PCI are consistent with the ITG turbulence, as expected for H-Mode plasmas before the ITB formation. The higher wavenumber part of the core turbulence is shifted toward higher frequencies by Doppler shift and is separated from the edge fluctuations. Under this circumstance, the measured fluctuation spectrum in the higher frequency band (above 300 kHz in the H-Mode plasma before the ITB formation) is dominated by core fluctuations and agrees with simulations. However, when the E×B Doppler shift is reduced, as in the ITB plasma, the core and edge turbulence overlaps. Consequently, although simulation in the core predicts weaker fluctuation intensity than the experimental measurements, this could be caused by significant contribution from the plasma edge and it may well dominate the larger wavelength spectrum ($k\rho_s < 1$).

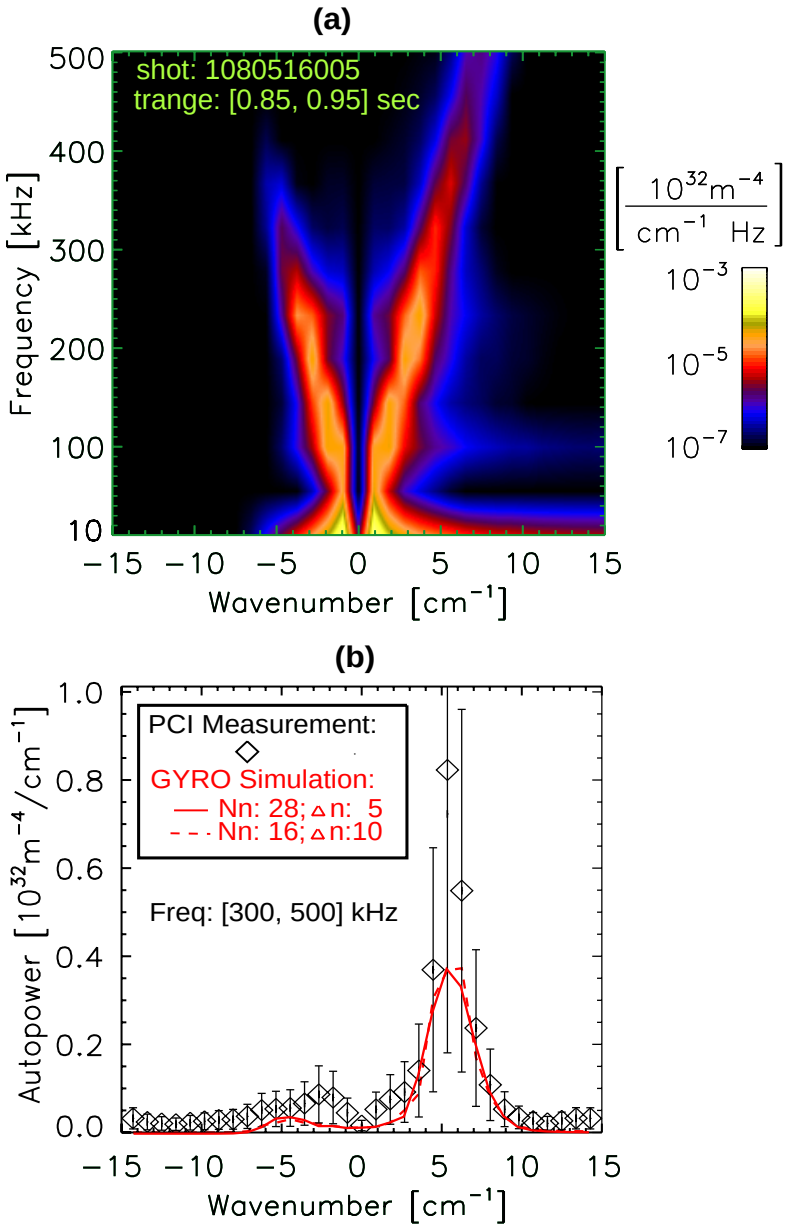


**Fig. 11.** (Color online). (a) Synthetic PCI frequency/wavenumber spectra in the H-Mode plasma before the ITB formation. A system response function has been implemented to emulate the top view configuration of the masked phase plate. (b) Comparison of the synthetic and experimental PCI wavenumber spectra integrated in the frequency range of 300-500 kHz.

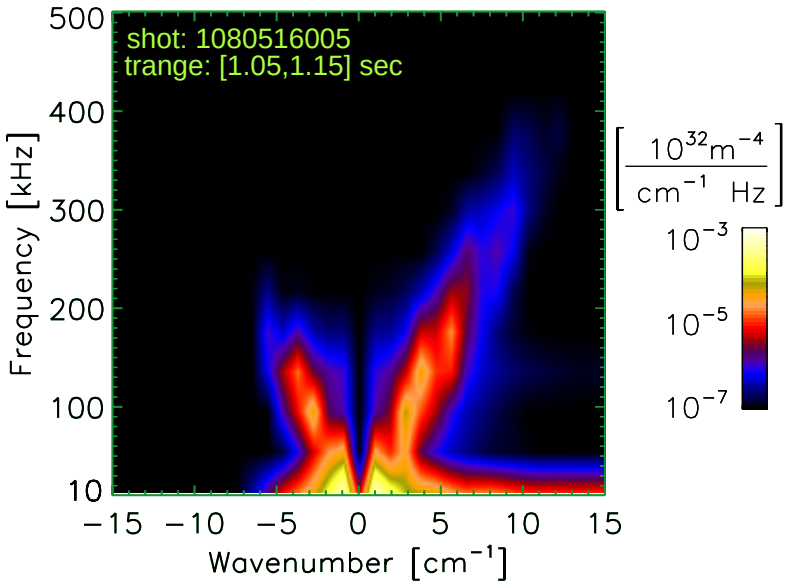


**Fig. 12.** (Color online). Synthetic PCI frequency/wavenumber spectra in the ITB with only off-axis ICRF heating. In the analysis, appropriate system response functions have been implemented to emulate the top view configuration of the masked phase plate.

## VI. Conclusions

In this paper, we have presented studies of turbulence and transport in the Alcator C-Mod H-Mode plasmas. The studies have included both experimental measurements of turbulence with the PCI diagnostic and numerical simulations of turbulence and transport with GYRO and good agreement is obtained in transport between code simulations and experiments after reducing the measured ion temperature gradient by ~15% and/or adding the ExB shear suppression, all within the experimental uncertainty. We have also compared the simulated level of turbulence from GYRO with the experimental measurements through a synthetic diagnostic. The simulated fluctuations agree with experimental measurements. Before the ITB formation, the fluctuations above 300 kHz are measured to be core-localized ($r/a<0.85$) and agree with the ITG spectrum in nonlinear GYRO simulations, including the direction of propagation, wavenumber spectrum, and absolute intensity, all within an experimental uncertainty. The fluctuation below 300 kHz is dominated by the edge turbulence and shows stronger fluctuation intensity than the GYRO simulation of the core. After the ITB formation, the reduced E×B Doppler shift causes a downshift of the core turbulence in frequency, which makes the core turbulence and edge turbulence spectrum overlaps on the PCI. Consequently, GYRO simulation in the core shows

overall weaker fluctuation intensity than experiments which also include contributions from the plasma edge, which may well dominate at sufficiently low frequencies.

## Acknowledgments

The authors want to thank Jeff Candy and Ron Waltz (General Atomics) for enlightening discussions and help with the GYRO simulations, Alexander C Ince-Cushman and John Rice (MIT PSFC) for providing the radial electric field measurements, Yunxing Ma and Jerry Hughes (MIT PSFC) for the Thomson scattering density and temperature profiles, and the Alcator C-Mod operations group for their support of this work.

This work is supported by U. S. DOE under DE-FG02-94-ER54235 and DE-FC02-99-ER54512. This research also utilized parallel computational clusters at MIT Plasma Science and Fusion Center (Loki) and Princeton Plasma Physics Laboratory (Kestrel).

## References

[1]J. Candy and R. E. Waltz, Phys. Rev. Lett. **91**, 045001 (2003).
[2]W. Dorland, F. Jenko, M. Kotschenreuther, and B. N. Rogers, Phys. Rev. Lett. **85**, 5570 (2000).
[3]F. Jenko, W. Dorland, M. Kotschenreuther, and B. N. Rogers, Phys. Plasmas **7**, 1904 (2000).
[4]Y. Chen and S. Parker, J. Comput. Phys. **220**, 839 (2007).
[5]Z. Lin, Y. Nishimura, Y. Xiao, I. Holod, W. L. Zhang, and L. Chen, Plasma Phys. Contr. Fusion **49**, B163-B172 (2007).
[6]R. V. Bravenec and W.M. Nevins, Rev. Sci. Instrum. 77, 015101 (2006).
[7]M. Porkolab, J.C. Rost, N. Basse, J. Dorris, E. Edlund, L. Lin, Y. Lin, and S. Wukitch, IEEE Trans. Plasma Sci. **34**, 229 (2006).
[8]N. P. Basse, E. M. Edlund, D. R. Ernst, C. L. Fiore, M. J. Greenwald, A. E. Hubbard, J. W. Hughes, J. H. Irby, L. Lin, Y. Lin, E. S. Marmar, D. A. Mossessian, M. Porkolab, J. E. Rice, J. A. Snipes, J. A. Stillerman, J. L. Terry, S. M. Wolfe, S. J. Wukitch, and K. Zhurovich, Phys. Plasmas **12**, 052512 (2005).
[9]D. R. Ernst, N. Basse, W. Dorland, C. L. Fiore, L. Lin, A. Long, M. Porkolab, K. Zeller, and K. Zhurovich, IAEA Fusion Energy Conference Chengdu, China, 16-21 October (2006), oral paper IAEA-CN-149/TH/1-3.
[10]N. Tsujii, M. Porkolab, E.M. Edlund, L. Lin, Am. Phys. Soc. **52** (16), 215 (2007).
[11]J.C. Rost, M. Porkolab, J.R. Dorris, J. Candy, KH. Burrell, Bull. Am. Phys. Soc. **52** (16), 334 (2007).
[12]C. L. Fiore, D. R. Ernst, J. E. Rice, K. Zhurovich, N. Basse, P. T. Bonoli, M. J. Greenwald, E. S. Marmar, S. J. Wukitch C. L. Fiore, D. R. Ernst, J. E. Rice, K. Zhurovich, N. Basse, P. T. Bonoli, M. J. Greenwald, E. S. Marmar, S. J. Wukitch, Fusion Sci. Technol., **51**, 303 (2007).
[13]M. Greenwald, D. Andelin, N. Basse, S. Bernabei, P. Bonoli, B. Böse, C. Boswell, R. Bravenec, B. Carreras, I. Cziegler, E. Edlund, D. Ernst, C. Fasoli, M. Ferrara, C. Fiore, R. Granetz, O.

Grulke, T. Hender, J. Hosea, D.H. Howell, A. Hubbard, J. Hughes, I. Hutchinson, A. Ince-Cushman, J. Irby, B. LaBombard, R. LaHaye, L. Lin, Y. Lin, B. Lipschultz, J. Liptac, S. Lisgo, A. Lynn, E. Marmar, K. Marr, D.R. Mikkelsen, R. McDermott, D. Mossessian, A. Parisot, R. Parker, C. Phillips, P. Phillips, M. Porkolab, M. Redi, J. Rice, W. Rowan, M. Sampsell, G. Schilling, S. Scott, J.T. Scoville, N. Smick, J. Snipes, P. Stangeby, V. Tang, J. Terry, M. Ulrickson, G. Wallace, D. Whyte, J. Wilson, J. Wright, S. Wolfe, S. Wukitch, B. Youngblood, H. Yuh, K. Zhurovich and S. Zweben, Nucl. Fusion **45,** S109 (2005).

[14]P. T. Bonoli, R. Parker, S. J. Wukitch, Y. Lin, M. Porkolab, J. C. Wright, E. Edlund, T. Graves, L. Lin, J. Liptac, A. Parisot, A. E. Schmidt, V. Tang, W. Beck, R. Childs, M. Grimes, D. Gwinn, D. Johnson, J. Irby, A. Kanojia, P. Koert, S. Marazita, E. Marmar, D. Terry, R. Vieira, G. Wallace, J. Zaks, S. Bernabei, C. Brunkhorse, R. Ellis, E. Fredd, N. Greenough, J. Hosea, C. C. Kung, G. D. Loesser, J. Rushinski, G. Schilling, C. K. Phillips, J. R. Wilson, R. W. Harvey, C. L. Fiore, R. Granetz, M. Greenwald, A. E. Hubbard, I. H. Hutchinson, B. LaBombard, B. Lipschultz, J. Rice, J. A. Snipes, J. Terry, S. M. Wolfe, Alcator C-Mod Team, Fusion Sci. Technol. **51**, 401 (2007).

[15]M. Greenwald, R. Boivin, P. Bonoli, R. Budny, C. Fiore, J. Goetz, R. Granetz, A. Hubbard, I. Hutchinson, J. Irby, B. LaBombard, Y. Lin, B. Lipschultz, E. Marmar, A. Mazurenko, D. Mossessian, T. Sunn Pedersen, C. S. Pitcher, M. Porkolab, J. Rice, W. Rowan, J. Snipes, G. Schilling, Y. Takase, J. Terry, S. Wolfe, J. Weaver, B. Welch, and S. Wukitch, Phys. Plasmas **6**, 1943 (1999).

[16] J.E. Rice, P.T. Bonoli, E.S. Marmar, S.J. Wukitch, R.L. Boivin, C.L. Fiore, R.S. Granetz, M.J. Greenwald, A.E. Hubbard, J.W. Hughes, I.H. Hutchinson, J.H. Irby, Y. Lin, D. Mossessian, M. Porkolab, G. Schilling, J.A. Snipes and S.M. Wolfe, Nucl. Fusion **42**, 510 (2002).

[17]C. L. Fiore, P. T. Bonoli, D. R. Ernst, A. E. Hubbard, M. J. Greenwald, A. Lynn, E. S. Marmar, P. Phillips, M. H. Redi, J. E. Rice, S. M. Wolfe, S. J. Wukitch, and K. Zhurovich, Phys. of Plasmas **11**, 2480 (2004).

[18]J. W. Hughes, D. Mossessian, K. Zhurovich, M. DeMaria, K. Jensen, and A. Hubbard, Rev. Sci. Instru., **74**, 1667 (2003).

[19]A. True, A. Quemeneur, P. Hennequin, D. Gresillon, and F. Gervais, Rev. Sci. Instrum. **63**, 3716 (1992).

[20]S. Kado, T. Irie, K. Muraoka, K. Matsuo, K. Tanaka, K. Kondo, F. Sano, and T. Obiki, Jpn. J. Appl. Phys. **34**, 6492 (1995).

[21]L. Lin, E.M. Edlund, M. Porkolab, Y. Lin, and S. J. Wukitch, Rev. Sci. Instrum. **77**, 10E918 (2006).

[22]J. R. Dorris, J.C. Rost, M. Porkolab, Rev. Sci. Instrum. to be published (2008).

[23]A. Mazurenko, M. Porkolab, D. Mossessian, J. A. Snipes, X.Q. Xu and W.M. Nevins, Phys. Rev. Lett. **89**, 225004 (2002).

[24]A. Ince-Cushman, J. E. Rice, S. G. Lee, M. Bitter, M. Reinke, and Y. Podpaly, Rev. Sci. Instrum. **77**, 10F321 (2006).

[25]R.J. Goldston, D.C. McCune, H.H. Towner, S.L. Davis, R.J. Hawryluk, and G.L. Schmidt, J. Comput. Phys. **43**, 61 (1981).

[26]C.L. Fiore and R. L. Boivin, Rev. Sci. Instrum. **66**, 945 (1995).

[27]R.E. Waltz, Private communications (2008).

[28]C. Holland, G.R. Tynan, G.R. McKee, M.W. Shafer, J. Candy, R.E. Waltz, R.V. Bravenec, Bull. Am. Phys. Soc. **52** (16), 334 (2007).

[29]J.E. Kinsey, R.E. Waltz and J. Candy, Phys. Plasma **14**, 102306 (2007).